Nanostructures

DOI: 10.1002/anie.200703175

Two-Dimensional Nanosheet Crystals**

*Jung-wook Seo, Young-wook Jun, Seung-won Park, Hyunsoo Nah, Taeho Moon, Byungwoo Park, Jin-Gyu Kim, Youn Joong Kim, and Jinwoo Cheon**

Two-dimensional crystals, which possess a nanoscale dimension only in the *c* axis and have infinite length in the plane, have been emerging as important new materials owing to their unique properties and potential applications in areas ranging from electronics to catalysis.[1–5] In particular, recent developments of 2D nanosheet crystals such as stable graphene and transition-metal chalcogenides (TMCs) have sparked new discoveries in condensed-matter physics and electronics.[6] Further miniaturization of these 2D structures by lateral confinements can potentially bring not only the modulation of electron-transport phenomena[7] but also the enhancement of their 2D host capabilities which arise from the enlarged surface area and improved diffusion processes upon the intercalation of guest molecules.[8] However, synthetic routes for such laterally confined 2D crystals, especially for TMCs, have been challenging since they are unstable and immediately scroll up into closed structures such as quasi-0D onions or 1D tubes owing to increased peripheral dangling bonds.[9–11]

Herein, we have developed an entirely new "shape-transformation" concept that proceeds by a rolling out of 1D tungsten oxide nanorods for the fabrication of laterally confined (less than 100 nm) 2D WS_2 nanosheet crystals. Here, a surfactant-assisted low-temperature (lower than 350 °C) solution process is also critical in stabilizing 2D nanosheet structures as opposed to conventional high-temperature (higher than 700 °C) gas–solid routes which yield only 0D or 1D structures.[12–14] Our 2D WS_2 nanosheet crystals are synthesized from tungsten oxide ($W_{18}O_{49}$) nanorods[15,16] in the presence of carbon disulfide in hot hexadecylamine solution.

Figure 1 a shows an overview of our shape-transformation scheme for the generation of 2D WS_2 nanosheet crystals from the tungsten oxide rods. The reaction between the carbon disulfide and hexadecylamine generates in situ hydrogen disulfide and hexadecylisothiocyanate via *N*-hexadecyldithiocarbamate as a transient species [Eq. (1); see also Figures S1 and S2 in the Supporting Information], and subsequent

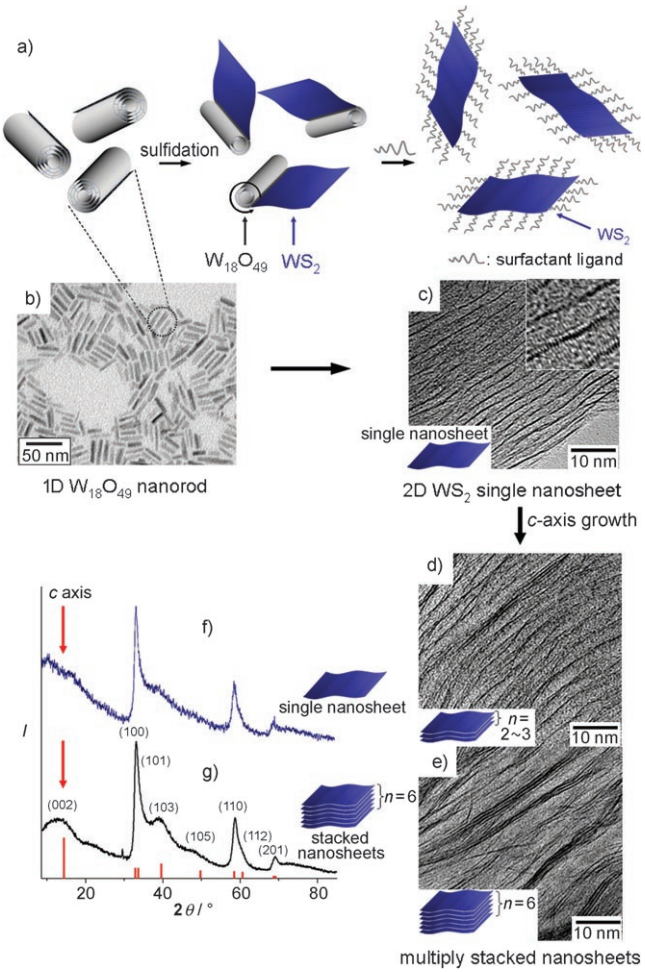

Figure 1. 2D WS_2 nanosheet crystal formation through rolling-out shape-transformation processes of 1D $W_{18}O_{49}$ nanorod precursors. a) Schematic diagram for the synthesis of 2D WS_2 nanosheet crystals. b) TEM image of $W_{18}O_{49}$ nanorod precursors. c–e) TEM images of 2D WS_2 obtained with the reaction times 10 min (c), 30 min (d), and 1 h (e) after the CS_2 injection. f) XRD analyses of the WS_2 single (top) and stacked (bottom) nanosheet crystals (red lines: JCPDS reference card no. 08-0237).

[*] J.-w. Seo, Y.-w. Jun, S.-w. Park, H. Nah, Prof. J. Cheon
Department of Chemistry
Yonsei University
Seoul 120-749 (Korea)
Fax: (+82) 2-364-7050
E-mail: jcheon@yonsei.ac.kr
T. Moon, Prof. B. Park
Department of Materials Science and Engineering
Seoul National University
Seoul 151-744 (Korea)
J.-G. Kim, Dr. Y. J. Kim
Division of Electron Microscopic Research
Korea Basic Science Institute
Daejeon 305-333 (Korea)

[**] This work was supported in part by the National Research Laboratory (NRL-2006-00457), NCRC (R15-2004-024-00000-0), second stage BK 21, KRF (2004-201-C00050), the ERC program of MOST/KOSEF (R11-2002-102-00000-0), and Samsung Electromechanics PhD training program.

Supporting information for this article is available on the WWW under http://www.angewandte.org or from the author.

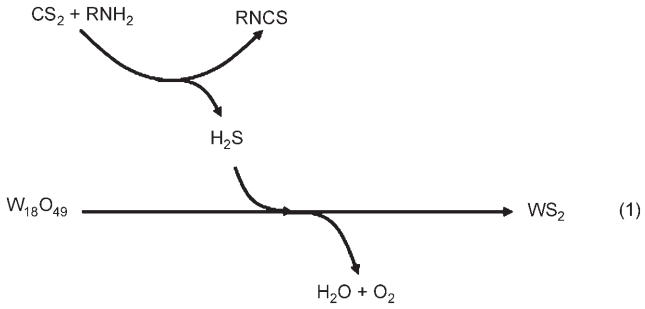

(1)

reaction between the 1D tungsten oxide rods and hydrogen disulfide leads to their sulfidation.[17,18]

As the sulfidation reaction proceeds, WS_2 is continuously unrolled to form a single-sheet structure from cylindrical tungsten oxide owing to the strains built from two heterogeneous phases. The resulting single sheets of 2D WS_2 further assemble together through van der Waals interactions to form stable bundles composed of multiple WS_2 single sheets. This process from single sheet to bundle formation is clearly observed by the transmission electron microscopic (TEM) images of 2D WS_2 obtained as the reaction proceeds (Figure 1c–e). After 1 h, the resulting 2D WS_2 nanosheet crystals are composed of approximately six single sheets (Figure 1e). The shape-transformation processes seem to be facilitated by the use of a nanoscale rod precursor with enhanced reactivity as compared to the bulk material.[19]

The XRD patterns support the TEM results. The overall shape of the peaks is asymmetric, which is a characteristic feature associated with 2D nanosheet structures.[20,21] While the (100) and (110) peaks for the *ab* plane are highly intense, the (002) peak for the *c* axis is either absent (arrow in Figure 1f, top) or weak (arrow in Figure 1f, bottom). This result indicates that our 2D nanosheet crystals produced at the initial stage are single sheets and are gradually assembled to form the multiply stacked structures.

Figure 2 shows a different view of the multiply stacked WS_2 nanosheet crystals, whereby both the vertically stacked sheets and planar shapes are observed. In general, viewing planar structures can be difficult because some structures are oriented parallel to the TEM grid while others are perpendicular. In our case, rotating the TEM holder stage along the [001] direction of the nanosheets shows that the vertically stacked sheets are indeed made up of stacked 2D sheets (Figure 2d–f). The overall size of the 2D WS_2 nanosheet crystals obtained is a length of 40 nm (standard deviation (σ) $\approx$16%) and a width of 35 nm ($\sigma\approx$14%) when precursor tungsten oxide nanorods with a length of 30 nm ($\sigma\approx$15%) and a diameter of 5 nm ($\sigma\approx$12%) are used.

The high-resolution TEM crystallographic analyses show vertically stacked nanosheet crystals composed of approximately six single WS_2 (002) layers with an interplanar spacing of 6.2 Å and periodic arrays of (100) planes with a spacing of 2.7 Å (Figure 2b). In the planar orientation, lattice fringes with interplanar spacings of 2.7 Å and 1.6 Å are clearly observed, corresponding to the (100) and (110) planes of the hexagonal (2H-type) WS_2, respectively (Figure 2c). Selected area electron diffraction (SAED) studies show patterns

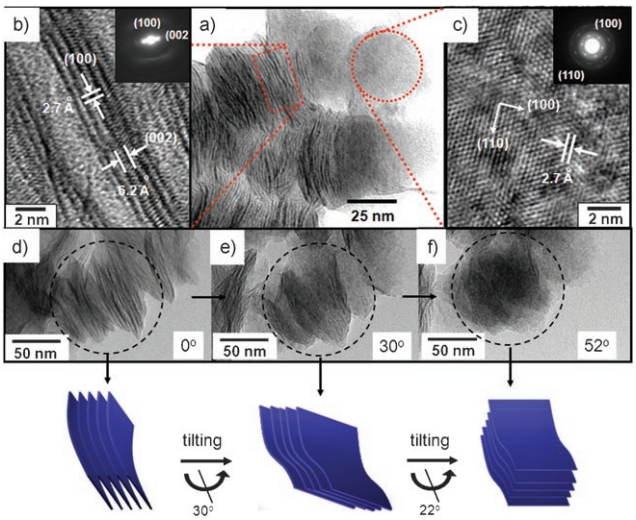

Figure 2. TEM analyses of 2D WS_2 nanosheet crystals. a) Low-magnification TEM image of 2D WS_2 nanosheet crystals ($n=6$). High-resolution TEM images of vertically aligned (b) and planar (c) nanosheet crystals. d)–f) TEM images obtained by rotating the TEM holder stage.

corresponding to the (002) and (100) reflections from the vertically stacked nanosheets and the (100) and (110) reflections of hexagonal WS_2 from planar nanosheets, respectively (insets of Figure 2b,c). Our analyses of WS_2 nanosheets with different orientations reveal these nanoparticles to be single-crystalline 2H-type WS_2 with hexagonal symmetry. Our proposed rolling-out mechanism is supported in part by the lateral size change of the 2D WS_2 nanosheet crystals when tungsten oxide nanorods with different lengths are used. When long tungsten oxide nanorods (ca. 75 nm) with a diameter of about 5 nm are used, the resulting 2D WS_2 nanosheet crystals have a length of about 85 nm (Figure 3a,b). The length in this case is roughly doubled compared to that of the nanosheets (ca. 40 nm) obtained from short tungsten oxide rods (ca. 30 nm) with the same diameter of about 5 nm (Figure 3c,d).

Owing to their unique morphologies of finite in-plane sizes (less than 100 nm) and well-defined layered structures, it is expected that laterally confined 2D nanosheet crystals can significantly enhance the host capabilities of active electrode materials. As opposed to the large planar structure of bulk WS_2, numerously divided modular 2D nanosheet crystals can possess excellent physicochemical properties arising from a highly enhanced surface area and easier accessibilities of guest molecules (Figure 4a). For example, the surface area of our 2D WS_2 nanosheet crystals is 37.2 $m^2 g^{-1}$, which is about 14.6 times higher than that of bulk WS_2 (2.5 $m^2 g^{-1}$), as determined by Brunauer–Emmett–Teller (BET) N_2 adsorption–desorption isotherms (see the Supporting Information, Figure S3). Such large surface area and the enhanced diffusion accessibility of Li ions through the widely open edges of the 2D nanosheet crystals make higher charge/discharge capacity possible (Figure 4a). When electrochemical properties of the nanosheet crystals were measured by fabricating coin-type half cells (2016 type) consisting of

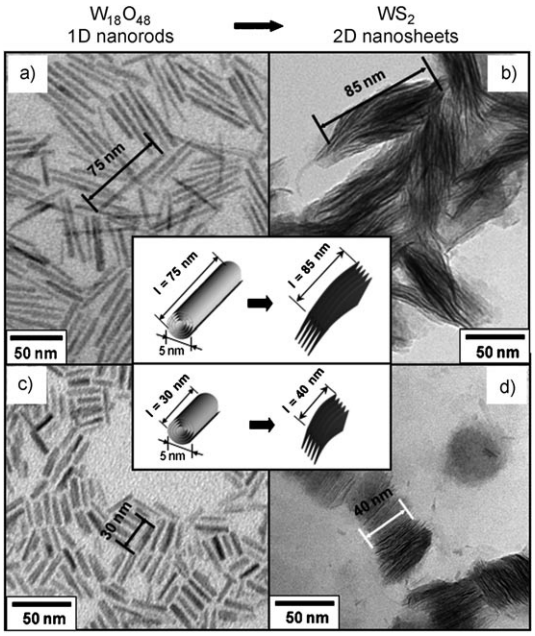

Figure 3. TEM images of two differently sized 2D WS_2 nanosheet crystals obtained by shape transformation of long (ca. 5 nm × 75 nm) and short (ca. 5 nm × 30 nm) tungsten oxide nanorods. Nanosheet crystals of about 85 nm in length (b) are obtained from long tungsten oxide nanorods (a), while nanosheet crystals of about 40 nm in length (d) are observed from short tungsten oxide nanorods (c).

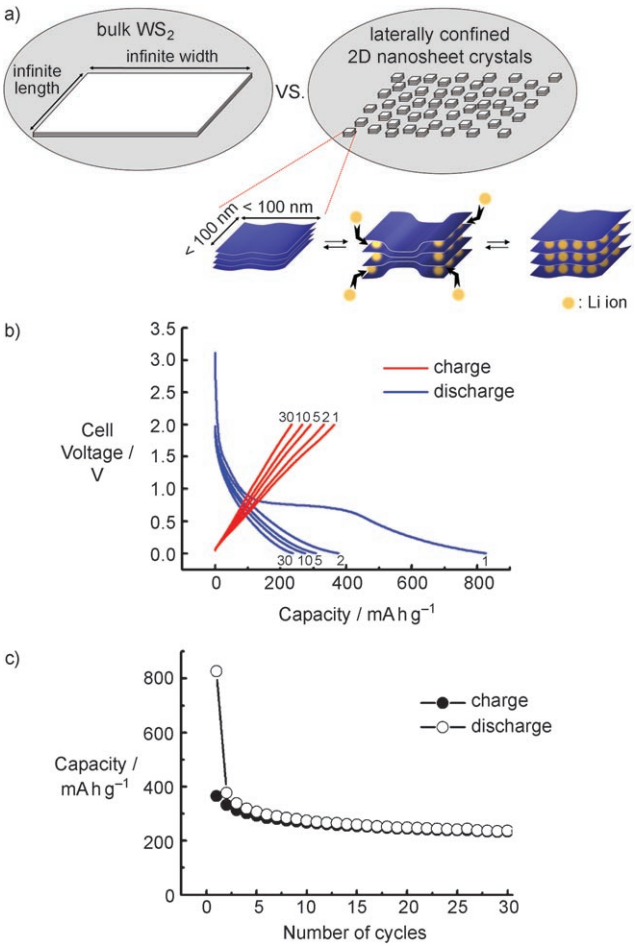

Figure 4. Electrochemical properties of 2D WS_2 nanosheet crystals for Li ion batteries. a) Schematic representation of the Li ion intercalation process in 2D WS_2 nanosheet crystals. b) Cell-voltage profiles of 2D WS_2 nanosheet crystals during the 1st, 2nd, 5th, 10th, and 30th cycles between 5 mV and 2.0 V. c) Cycle-life performance (charge (●) and discharge (○) vs. cycle number) of the 2D WS_2 nanosheet crystals, which is cycled up to the 30th cycle under constant-current conditions (100 mA g^{-1}).

80 wt% 2D WS_2 nanosheet crystals, the first reversible discharge capacity was 377 mA h g^{-1}, corresponding to an intercalation of 3.5 mol of lithium ions per mol of WS_2 (Figure 4b). Our nanosheet crystals show highly reversible electrochemical properties and stable cycling performance in 30 tested cycles (Figure 4c). Also, the observed discharge capacity of 2D nanosheet crystals is significantly higher (ca. 5.8 times) than that of bulk WS_2.[22]

In summary, we have developed a unique, simple, and versatile shape-transformation route which can provide high-quality 2D nanosheet crystals with nanoscale lateral dimensions (less than 100 nm). Along with a large surface area, the finite lateral size and enhanced open-edge morphology of the 2D nanosheet crystals play a significant role in retaining a higher intercalation capacity, which enables them to be excellent electrode materials. Our 2D nanosheet crystals can be useful as swellable modular host materials for various applications requiring a large density and fast intercalation processes, including host–guest intercalations, high-performance catalysis, and energy storage.

Experimental Section

Materials and instruments: All chemicals were purchased from Aldrich and all were used as received. Tungsten oxide nanorods were prepared following methods in the literature.[15,16] TEM and high-resolution TEM analyses were performed on a JEOL-JEM 2100 at 200 kV or on a JEOL-ARM1300S at 1250 kV. X-ray diffraction studies were conducted using a Rigaku D/MAX-RB equipped with a graphite-monochromated $Cu_{K\alpha}$ radiation source (40 kV, 120 mA). Mass spectrometry and GC–MS of reaction by-products were conducted on a Finnigan MAT 271 and JEOL-JMS600 (EI+ mode). The surface area of the 2D WS_2 nanosheet crystals was measured on an ASAP 2400 (Micromeritics, N_2 gas).

Synthesis of 2D WS_2 nanosheet crystals: Tungsten oxide nanorods (40 mg) and hexadecylamine (1.45 g, 6 mmol) were added to a 50-mL three-neck round-bottom flask under argon. The reaction mixture was first heated to 100 °C for 1 hr in vacuum to remove impurities such as water, and then was subsequently heated to 250 °C. The sulfidation reaction was initiated by injecting carbon disulfide (0.12 mL, 2 mmol), and the resulting solution was further heated to 330 °C. During the reaction, the initially blue solution gradually became dark brown, and the reaction was stopped by removing the heating source after 1 hr. Variation of the growth time (e.g. 10 min and 30 min) was also performed to obtain single- and multiple-layered (2–3 layers) nanosheet crystals, respectively. The resulting solution was cooled to room temperature and treated with acetone (20 mL) to precipitate dark brown nanoparticles (26 mg) which were then redispersed in toluene (5 mL). The obtained nanoparticles possess high colloidal stability in various organic solvents such as toluene, hexane, and dichloromethane over one month. With the same experimental procedures, a scaled-up synthesis of 2D WS_2 nanosheet crystals was performed using tungsten oxide nanorods (400 mg), hexadecylamine (7.24 g, 30 mmol), and CS_2 (0.6 mL,

10 mmol). The scaled-up procedure produced approximately 240 mg of the WS_2 nanosheet crystals.

Electrochemical properties of 2D WS_2 nanosheet crystals: Cycling tests were performed using coin-type half cells (2016 type) with a Li counterelectrode. WS_2 nanosheet crystals were annealed before use at 750 °C for 1 h to remove any organic species. The working electrode was composed of 80 wt % WS_2 nanosheet crystals, 10 wt % Super P carbon black, and 10 wt % polyvinylidene fluoride. A solution of $LiPF_6$ (1 M) in ethylene carbonate/diethylene carbonate (1:1 v/v) was used as the electrolyte. The cells were discharged from the initial open-circuit voltage to 5 mV, and cycled between 5 mV and 2 V after the first discharge. The cycling tests were performed under constant-current conditions (100 mA g^{-1}) for up to 30 cycles.

Received: July 16, 2007
Published online: October 15, 2007

Keywords: electrochemistry · intercalations · nanosheets · nanostructures · transmission electron microscopy

[1] K. S. Novoselov, A. K. Geim, S. V. Morozov, D. Jiang, M. I. Katsnelson, I. V. Grigorieva, S. V. Dubonos, A. A. Firsov, *Nature* **2005**, *438*, 197 – 200.
[2] K. S. Novoselov, D. Jiang, F. Schedin, T. J. Booth, V. V. Khotkevich, S. V. Morozov, A. K. Geim, *Proc. Natl. Acad. Sci. USA* **2005**, *102*, 10451 – 10453.
[3] N. A. Dhas, K. S. Suslick, *J. Am. Chem. Soc.* **2005**, *127*, 2368 – 2369.
[4] L. M. Viculis, J. J. Mack, R. B. Kaner, *Science* **2003**, *299*, 1361.
[5] Y. Zhang, Y.-W. Tan, H. L. Stormer, P. Kim, *Nature* **2005**, *438*, 201 – 204.
[6] A. K. Geim, K. S. Novoselov, *Nat. Mater.* **2007**, *6*, 183 – 191.
[7] R. Mu, Y. S. Tung, A. Ueda, D. O. Henderson, *J. Phys. Chem.* **1996**, *100*, 19927 – 19932.
[8] F. Levy, *Intercalated Layered Materials*, 1st ed., D. Reidel, Boston, **1940**.
[9] R. Tenne, *Adv. Mater.* **1995**, *7*, 965 – 995.
[10] Y. D. Li, X. L. Li, R. R. He, J. Zhu, Z. X. Deng, *J. Am. Chem. Soc.* **1998**, *120*, 6189 – 6190.
[11] R. Tenne, *Nat. Nanotechnol.* **2006**, *1*, 103 – 111.
[12] Y. Feldman, E. Wasserman, D. J. Srolovitz, R. Tenne, *Science* **1995**, *267*, 222 – 225.
[13] M. Remskar, A. Mrzel, Z. Skraba, A. Jesih, M. Ceh, J. Demšyar, P. Stadelmann, F. Lévy, D. Mihailovic, *Science* **2001**, *292*, 479 – 481.
[14] A. Rothschild, J. Sloan, R. Tenne, *J. Am. Chem. Soc.* **2000**, *122*, 5169 – 5179.
[15] J.-w. Seo, Y.-w. Jun, S. J. Ko, J. Cheon, *J. Phys. Chem. B* **2005**, *109*, 5389 – 5391.
[16] K. Lee, W. S. Seo, J. T. Park, *J. Am. Chem. Soc.* **2003**, *125*, 3408 – 3409.
[17] M. Ballabeni, R. Ballini, F. Bigi, R. Maggi, M. Parrini, G. Predieri, G. Sartori, *J. Org. Chem.* **1999**, *64*, 1029 – 1032.
[18] A. J. van der Vlies, G. Kishan, J. W. Niemantsverdriet, R. Prins, T. Weber, *J. Phys. Chem. B* **2002**, *106*, 3449 – 3457.
[19] Y. Li, H. Zhong, R. L. Yi, Y. Zhou, C. Yang, Y. Li, *Adv. Funct. Mater.* **2006**, *16*, 1705 – 1716.
[20] R. A. Gordon, D. Yang, E. D. Crozier, D. T. Jiang, R. R. Frindt, *Phys. Rev. B* **2002**, *65*, 125407.
[21] D. Yang, S. Jiménez Sandoval, W. M. R. Divigalpitiya, J. C. Irwin, R. F. Frindt, *Phys. Rev. B* **1991**, *43*, 12053 – 12056.
[22] C. M. Julien, *Mater. Sci. Eng. R* **2003**, *40*, 47 – 102.

